The Journal of Infectious Diseases

SUPPLEMENT ARTICLE

New Insights Into Marburg Virus Disease Pathogenesis in the Rhesus Macaque Model

Timothy K. Cooper, Jennifer Sword, Joshua C. Johnson, Amanda Bonilla, Randy Hart, David X. Liu, John G. Bernbaum, Kurt Cooper, Peter B. Jahrling, and Lisa E. Hensley

Integrated Research Facility at Fort Detrick, National Institute of Allergy and Infectious Diseases, National Institutes of Health, Fort Detrick, Frederick, Maryland

Previously, several studies have been performed to delineate the development and progression of Marburg virus infection in nonhuman primates (NHPs), primarily to clarify the mechanisms of severe (fatal) disease. After the 2013–2016 Ebola virus disease (EVD) epidemic in Western Africa, there has been a reassessment of the available filovirus animal models and the utility of these to faithfully recapitulate human disease. The high lethality of the NHP models has raised doubts as to their ability to provide meaningful data for the full spectrum of disease observed in humans. Of particular interest are the etiologic and pathophysiologic mechanisms underlying postconvalescent sequelae observed in human survivors of EVD and Marburg virus disease (MVD). In the current study, we evaluated the lesions of MVD in NHPs; however, in contrast to previous studies, we focused on the potential for development of sequelae similar to those reported in human survivors of MVD and EVD. We found that during acute MVD in the macaque model, there is frequent inflammation of peripheral nerves, autonomic ganglia, and the iris of the eye. Furthermore, we demonstrate viral infection of the ocular ciliary body and retina, testis, epididymis, ovary, oviduct, uterine endometrium, prostate, and mammary gland. These findings are relevant for both development of postconvalescent sequelae and the natural transmission of virus.

Keywords. Eye; anterior uveitis; nerve; ganglion; genital; mammary; Schwann cell; sequelae.

The family Filoviridae contains several etiologic agents of human viral hemorrhagic disease with high lethality, including Marburg virus (MARV) and Ebola virus (EBOV) [1]. Although long-term post–filovirus infection sequelae in recovered individuals had been described as early as the initial 1967 outbreak of MARV disease (MVD) in Europe, the unprecedented 2013–2016 EBOV disease (EVD) epidemic in Western Africa resulted in >10 000 EVD survivors, greatly increasing our awareness of postconvalescent complications [2–4]. Many of these survivors may need convalescent and long-term medical attention for their postinfection complications [5, 6]. Reported sequelae include (but are not limited to) arthralgia, uveitis, retinal and optic nerve disease, headache, and peripheral neuropathy [6–8]. Little is known regarding the underlying cause or the pathologic mechanism associated with many of these symptoms. This gap in knowledge has increased interest in understanding the mechanisms underlying filovirus disease sequelae and viral recrudescence.

MARV, the first identified filovirus, also has the potential for producing a large-scale outbreak of viral hemorrhagic fever [9]. Researchers suspect that a common species of fruit bat (*Rousettus aegyptiacus*) is the natural MARV reservoir [10]. The wide-range geographic distribution of these animals is reason for concern when determining the potential risk of a large-scale outbreak of MVD, which was first reported in 1967 in Marburg, Germany, and Belgrade, Yugoslavia (now Serbia), in laboratory workers who had been exposed to infected African green monkeys or their tissues [11, 12]. The largest outbreak of MVD was reported in 2005 in Angola, with a total of 374 confirmed cases and a case fatality rate of 88%; this outbreak was the largest filovirus outbreak on record until the 2013–2016 West Africa EVD epidemic [9, 13, 14].

Clinical manifestations, viral cell tropism, and the pathology of MVD parallel those of EVD [15]. Virus transmission occurs primarily through mucosal surfaces and breaks in the skin that come in contact with infected human or animal tissues and body fluids [1]. Sexual transmission of the disease has been reported, as well as exposure through breast milk [16, 17]. The incubation period for MVD ranges from 2 to 21 days before symptom onset. There are initial influenzalike symptoms during the generalization phase, followed by mucosal hemorrhage, visceral hemorrhage, dyspnea, petechiae, and edema in the early organ phase [18]. The late organ phase starts around day 13 after symptom onset and can include symptoms such as shock, diffuse coagulopathy, dementia, coma, convulsions, and multiorgan failure. In those who succumb to the disease, death typically occurs 8–16 days after disease onset [12, 16, 19]. Much less is known about MVD survivors, a gap that may be due to a limited number

Presented in part: Ninth International Filovirus Symposium, Marburg, Germany, 13–16 September 2017.

Correspondence: T. K. Cooper, DVM, PhD, DACVP, Integrated Research Facility at Fort Detrick, Division of Clinical Research, National Institute of Allergy and Infectious Diseases, National Institutes of Health, B-8200 Research Plaza, Fort Detrick, Frederick, MD 21702 (timothy.cooper@nih.gov).

The Journal of Infectious Diseases® 2018;218(S5):S423–33

DOI: 10.1093/infdis/jiy367

of survivors and lack of monitoring of those who have survived. From the limited available information, survivors of MVD may develop postconvalescent complications, such as myalgia, arthralgia, hepatitis, asthenia, ocular disease, and psychosis [2, 3, 20].

With an as-yet-undetermined incidence of sequelae after MVD it is important to understand the mechanisms behind postconvalescent complications. Using the established filovirus nonhuman primate (NHP) model to investigate postfilovirus disease sequelae would be advantageous, but MARV infection in this model is highly lethal, and survivors are rare. Given the challenges of developing a survivor model in NHPs, we are using the established filovirus NHP model to increase our knowledge of postfilovirus syndrome by looking at the critical target organs that may contribute to sequelae during the acute phase of the disease. We found that during acute MVD in the rhesus macaque model there was frequent inflammation of peripheral nerves, autonomic ganglia, and the anterior uvea, with viral infection of the ocular ciliary body and retina, male and female genital tract, and mammary gland. These findings are relevant for both potential development of postconvalescent sequelae and natural transmission of virus.

MATERIALS AND METHODS

Animals and Virus

Four female (4.0–5.2 years of age, NHP1-4) and 2 male (5.2 years of age, NHP5-6) Chinese-origin rhesus macaques (*Macaca mulatta*) were acclimatized to the maximum containment (biosafety level 4) laboratory at the US National Institutes of Health (NIH)/National Institute of Allergy and Infectious Diseases (NIAID)/Division of Clinical Research (DCR)/Integrated Research Facility at Fort Detrick (IRF-Frederick). After acclimatization, macaques were infected by the intramuscular route with a target dose of 1000 plaque-forming units of Marburg virus/H.sapiens-tc/AGO/2005/Ang-1379v (BioSample identifier SAMN05916381; henceforth, MARV), passage Vero E6p4. Exposure dose was confirmed to be approximately 856 plaque-forming units by means of a 2.5% Avicel 591 (RC-591 NF, FMC Biopolymer) plaque assay method, performed as described elsewhere [21].

Ethics Statement

Studies were performed in accordance with animal study protocols approved by an Animal Care and Use Committee of NIAID Division of Clinical Research, part of the National Institutes of Health. Protocols are compliant with the US Department of Agriculture Animal Welfare Act regulations and the US Public Health Service Policy on the Humane Care and Use of Laboratory Animals and adhere to the recommendations stated in *The Guide for the Care and Use of Laboratory Animals* [22]. All work with infectious virus was conducted in a biosafety level 4 laboratory at IRF-Frederick that is fully accredited by the Association for the Assessment and Accreditation of Laboratory Animal Care International.

Clinical Pathology

Serum chemistry was performed using a Piccolo General Chemistry 13 reagent disc on a Piccolo Xpress chemistry analyzer (Abaxis Medical), according to the manufacturer's instructions. Complete blood cell counts were performed using an XS-1000i hematology analyzer (Sysmex).

Necropsy and Histology

Macaques were humanely euthanatized in accordance with defined experimental end points that included observations and scoring by comparative medicine staff and, in consultation with the study veterinarian, evaluation of overall clinical appearance, respiratory rate, mucosal membrane appearance, dyspnea, recumbency, nonresponsiveness, and core temperature. Based on the total clinical score determined by assessing each these parameters for each NHP 3 times a day, and with the concurrence of veterinary staff, or at veterinary discretion, animals in this study reached criteria end points on postinfection days (PIDs) 7, 8, and 9, and gross necropsy was performed after euthanasia. Tissue fixation, embedding, sectioning, staining, and imaging for histology were performed as described elsewhere [23].

Immunohistochemistry

MARV immunohistochemistry (IHC) was performed with an antiglycoprotein (MARV glycoprotein [GP], 1:3000; rabbit polyclonal; IBT Bioservices catalog No. 0303-007) or antimatrix protein (VP40, 1:3000; mouse monoclonal; IBT Bioservices catalog No. 0203-012) primary antibody, followed by a biotinylated antirabbit secondary antibody (catalog No. 111-065-144; Jackson Immunoresearch Laboratories) or antimouse secondary antibody (catalog No. 115-065-166; Jackson Immunoresearch Laboratories) and an avidin-biotin peroxidase tertiary antibody (catalog No. PK-6100; Vector Laboratories). For tissues other than eye, staining was visualized with 3,3'-diaminobenzidine (brown) chromogen (catalog No. BDB2004L; Biocare Medical) and counterstained with hematoxylin. Because of the native brown melanin pigment in the uveal tract, eyes were stained with a blue chromogen, p-nitroblue tetrazolium chloride/5-bromo-4-chloro-3-indolyl phosphate (catalog No. 34042; Thermo Fisher Scientific) and nuclear fast red counterstain. Each section was stained with both GP and VP40 primary antibodies.

In Situ Hybridization

To detect MARV genomic RNA in formalin-fixed paraffin-embedded tissues, in situ hybridization (ISH) was performed using the RNAscope 2.5 HD RED kit (Advanced Cell Diagnostics), according to the manufacturer's instructions. Briefly, 20 ZZ probe pairs targeting the MARV genomic nucleoprotein (NP), VP35, and VP40 genes were used (Advanced Cell Diagnostics; catalog

No. 463751). Antigenomic positive sense single stranded RNA (ssRNA$^+$) was detected with complementary probes targeting the same genes (catalog No. 527301). After deparaffinization with xylene, a series of ethanol washes and peroxidase blocking, sections were heated in target retrieval buffer and then digested by proteinase. Sections were exposed to ISH target probe and incubated at 40°C in a hybridization oven for 2 hours. After rinsing, the ISH signal was amplified using company-provided preamplifier and amplifier conjugated to horseradish peroxidase, followed by incubation with a red substrate-chromogen solution for 10 minutes at room temperature. Sections were then counterstained with hematoxylin, dehydrated, and coverslipped.

Electron Microscopy

Fixation, embedding, sectioning, staining, and imaging for conventional thin-section transmission electron microscopic (TEM) evaluation of liver, spleen, ovary/testis, and prostate/uterus were performed as described elsewhere [24].

RESULTS

The clinical course, viral titers, serum chemistry changes, and findings in the liver, spleen, and lymph nodes, including gross and histologic lesions, ultrastructural examinations, IHC, and genome and antigenome ISH, were all fully consistent with previous descriptions of experimental intramuscular MARV Angola infection in the rhesus macaque model (Supplementary Figures 1–3 and data not shown) [25, 26]. Serum chemistry changes included increasing levels of alanine aminotransferase, aspartate aminotransferase, alkaline phosphatase, γ-glutamyltransferase, total bilirubin, creatinine, and serum urea nitrogen and decreasing levels of albumin and total protein. In addition, consistent with previous studies, there was positive immunostaining for viral proteins and ISH for viral genome in the pancreatic islets of Langerhans and adrenal cortex and medulla.

Eye

Three of 6 animals (at PIDs 7, 8, and 9) had several small perivascular infiltrates of activated macrophages admixed with necrotic cellular debris into the stroma of the iris, with occasional minimal to mild focal edema (Figure 1A and Supplementary Table 1). Inflammatory foci in the iris stained positively for MARV GP and VP40 antigen expression by IHC (Figure 1B, 5 of 6 animals) and for viral genome by ISH (Figure 1C, 5 of 6). In 5 of 6 animals, multiple capillaries and small veins within the choroid, ciliary body, and iris (uvea) were partially to completely occluded and sometimes expanded by emboli consisting of degenerate or necrotic vacuolated macrophages. These emboli were positive for both GP and VP40, as well as MARV genome.

The remaining ocular globe was unremarkable by routine histologic examination. By IHC, there was multifocal positive staining for GP and VP40 in the stroma (5 of 6 animals) and epithelium (4 of 6) of the ciliary body (Figure 1D). In a single animal, multifocal positive immunostaining was present in the smooth muscle cells of the ciliary body. The stromal fibroblasts of the ciliary body were positive for MARV genome in all 6 animals, with positive ciliary epithelial staining in 4 (Figure 1E). Mature virus particles were identified in the ciliary stroma by TEM, with viral replication within ciliary body endothelium (data not shown). In 2 animals (both at PID 8) there was multifocal positive hybridization in the smooth muscle cells of the ciliary body. There was also positive antigen staining of the endothelial cells lining the trabeculae of the drainage angle and Schlemm's canal (3 of 6 animals), and positive staining of the bulbar conjunctival epithelium and stroma (2 of 6). Remarkably, in 2 animals (both at PID 8; 1 with ciliary smooth muscle staining) there were several discrete small foci of positive genome staining in the inner nuclear layer of the retina (Figure 1F). Antigenome ISH staining was similar for all ocular structures (data not shown). All 6 animals had positive findings by viral reverse-transcriptase polymerase chain reaction analysis of the vitreous humor (data not shown).

Peripheral Nerves and Ganglia

In 5 of 6 macaques (all animals except 1 male euthanized on PID 8 [NHP5]), 1 to several sections of small to medium myelinated peripheral nerve had lesions ranging from occlusion of capillaries within the perineurium by degenerate and necrotic vacuolated macrophages to extravascular infiltrates of viable vacuolated macrophages. In some axons, there were occasional foci of intraneural hemorrhage and necrosis (Figure 2A). Peripheral parasympathetic autonomic ganglia were incidentally collected in multiple animals, including the periductal parasympathetic submandibular (Langley's) ganglion in 2 animals. In 3 animals (NHP2, NHP4, and NHP5), a spectrum of lesions similar to those present in the nerves above were also present in the parasympathetic ganglia (Figure 2B).

Within peripheral nerves, positive staining of intravascular and infiltrating macrophages for GP and VP40 antigens was present, as well as within foci of necrosis and inflammation affecting the axons (Figure 2C). Multifocally neurofibroblasts and Schwann cells were also positive. In the ganglia, low numbers of infiltrating macrophages were positive by immunostaining, with nearly diffuse staining of the interstitial neurofibroblasts and Schwann cells (Figure 2D). With ISH, viral genome and antigenome was demonstrated within infiltrating macrophages, neurofibroblasts, and Schwann cells in the peripheral nerves (Figure 2E) and ganglia (Figure 2F). Ganglion cells (neurons), satellite cells, and nerve axons were uniformly negative by IHC and ISH. For all animals, multiple sections of brain (including cerebral cortex, cerebellum and brain stem) were reviewed; there were no significant findings.

Gonads and Genital Tract

In 3 of 4 female macaques (NHP1, NHP2, and NHP4; PIDs 7, 8 and 9), there was scattered degeneration and necrosis of the

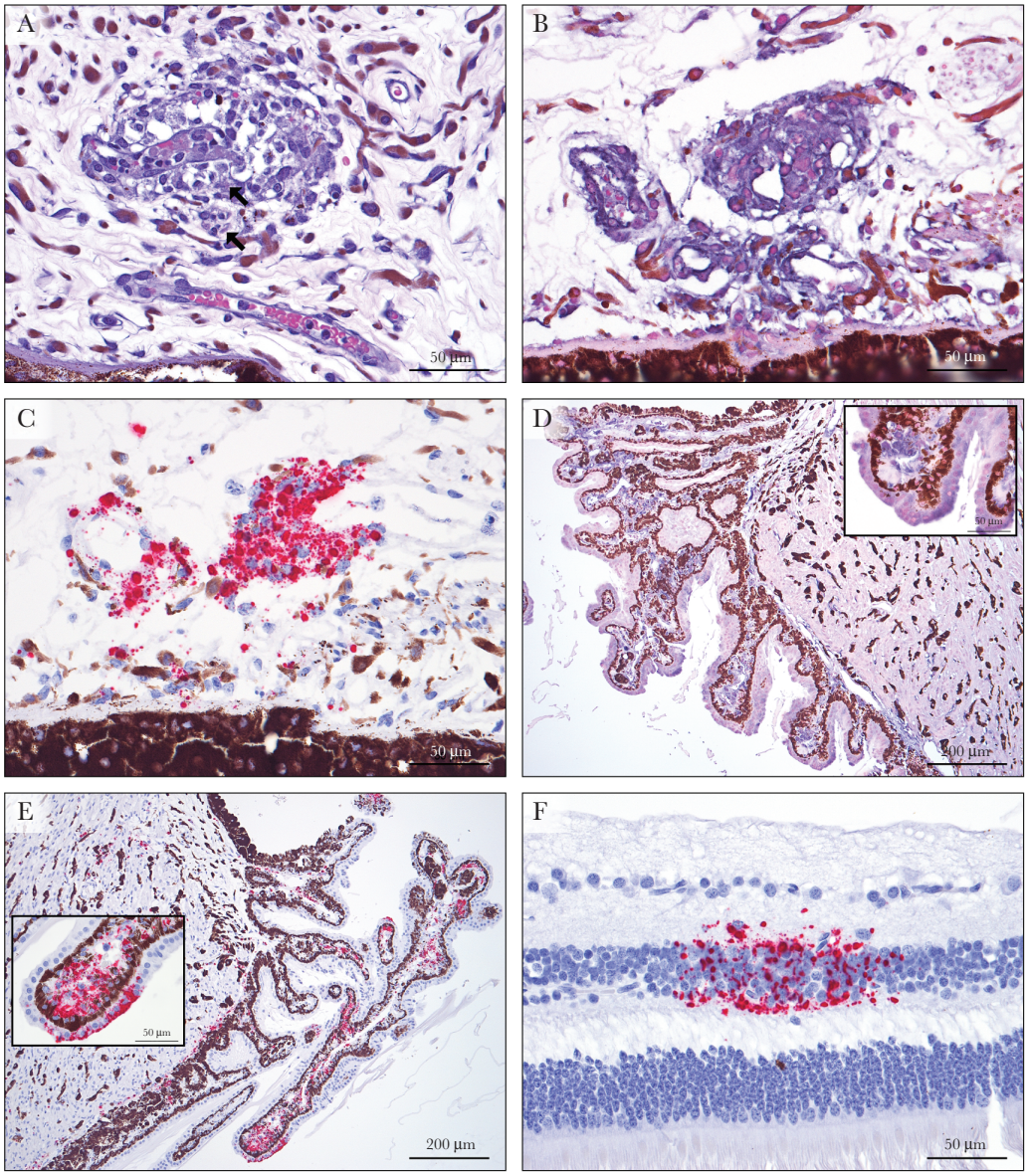

Figure 1. Histopathology of the eye in Marburg virus (MARV) infection. *A*, A venule in the iris is partially occluded by an embolus of viable, degenerate, and necrotic vacuolated macrophages, with infiltration of macrophages into the surrounding perivascular stroma and mild edema. There are rare viral intracytoplasmic inclusion bodies (*arrows*) (hematoxylin-eosin staining). *B,* Immunolabeling for MARV glycoprotein (GP) is positive in intravascular and extravascular macrophages and interstitial fibroblasts in the iris (nitroblue tetrazolium and 5-bromo-4-chloro-3-indolyl-phosphate chromagen and hematoxylin counterstain). *C,* MARV genome in situ hybridization (ISH) labels iridial fibroblasts and intravascular and extravascular macrophages, with scattered non–cell-associated staining (red substrate chromagen and hematoxylin counterstain). *D,* Positive immunostaining for MARV GP is present in morphologically normal ciliary body epithelium, stromal fibroblasts, and smooth muscle cells. Inset shows higher magnification of positive ciliary epithelium and stroma. *E,* Positive ISH findings for MARV genome in the epithelial cells, smooth muscle, and stroma of the ciliary body. Inset shows higher magnification of ciliary epithelium and stroma. *F,* Discrete foci of MARV genomic RNA are present in the inner nuclear layer of the retina.

circumferential stromal cells surrounding secondary and tertiary follicles (theca interna), with rare viral intracytoplasmic inclusion bodies. The theca interna cells were strongly and diffusely positive for GP and VP40 antigen in all 4 females, with scattered clusters of interstitial ovarian stromal cells between follicles (Figure 3A). In a single female macaque (NHP3), positive staining in clusters of granulosa cells in secondary and tertiary follicles was present. ISH showed similar results (Figure 3B). By ultrastructural examination, viral nucleocapsids forming cytoplasmic tubular and granular inclusions were present in interstitial stromal cells and theca interna cells, and as mature free virus particles. Infection of granulosa cells was confirmed in NHP3. The fourth female macaque was sexually immature, with rare secondary follicles.

In 1 macaque (NHP1), foci of necrosis and hemorrhage replaced the endosalpingeal epithelium of the oviductal fimbriae. All 4 females had positive findings of immunostaining

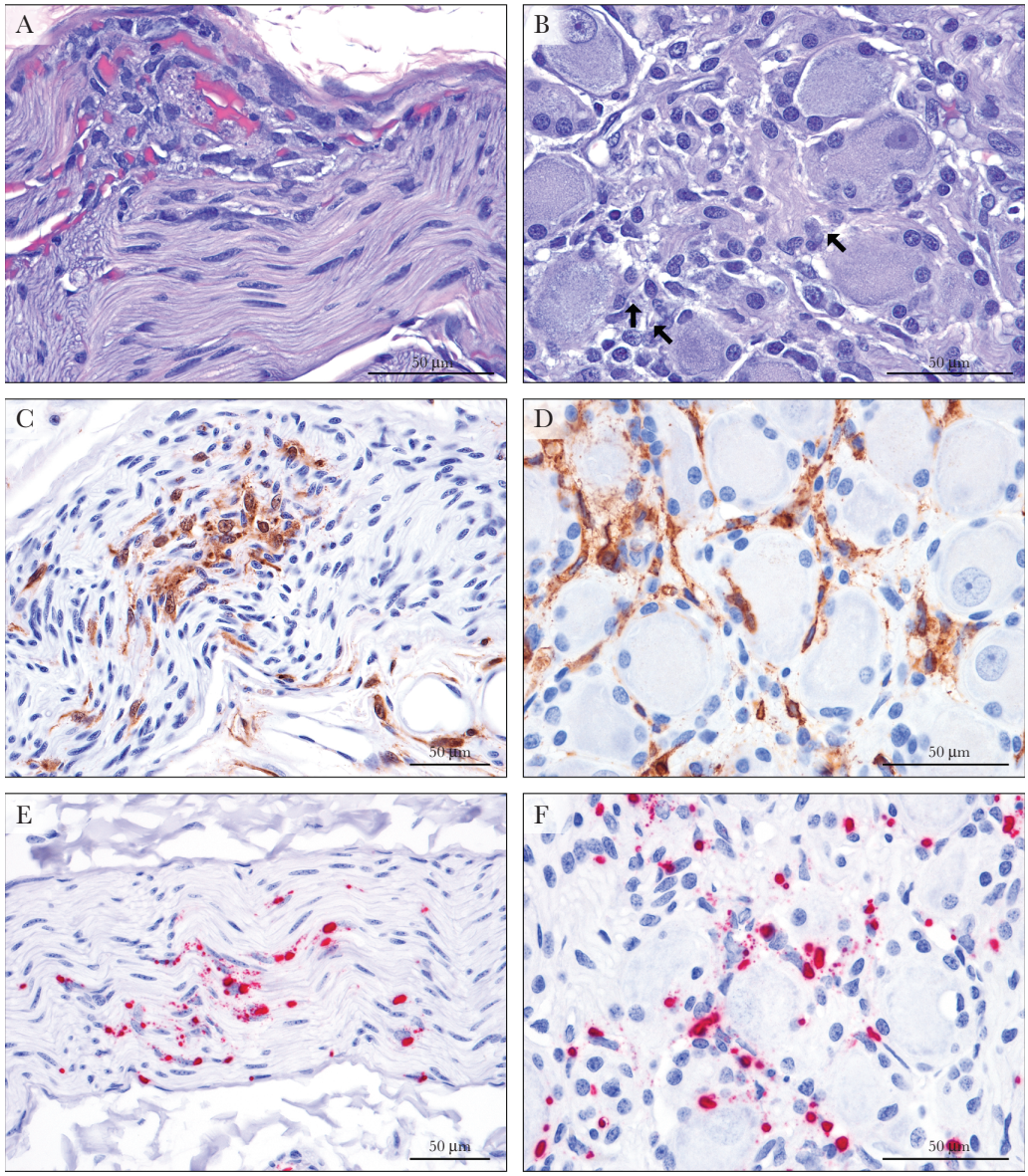

Figure 2. Histopathology of peripheral myelinated nerves and ganglia in Marburg virus (MARV) infection. *A,* In a peripheral medium myelinated nerve, focal hemorrhage and histiocytic inflammation with necrotic cell debris dissecting between axons was present. *B,* Within the submandibular (Langley's) parasympathetic autonomic ganglion, macrophages infiltrate and expand between ganglion cells, with necrotic cellular debris. There are rare viral intracytoplasmic inclusion bodies (*arrows*) (hematoxylin-eosin staining). *C,* Immunostains for MARV matrix protein label infiltrating macrophages, supporting Schwann cells, and neurofibroblasts (3,3′-diaminobenzidine [DAB] chromagen and hematoxylin counterstain). *D,* Infiltrating macrophages, supporting Schwann cells and neurofibroblasts express MARV glycoprotein in the ganglion. *E, F,* In situ hybridization for MARV genome labels infiltrating macrophages, supporting Schwann cells, and neurofibroblasts in the nerve (*E*) and ganglion (*F*) (red substrate chromagen and hematoxylin counterstain).

and ISH in the epithelial cells (and stroma) of the fimbriae of the oviduct (Figure 3C and D). In NHP1 there were also clusters of IHC- and ISH-positive smooth muscle cells in the myosalpinx (Figure 3E and F).

In a single female (NHP2), low to moderate numbers of vacuolated, apoptotic, and inclusion-bearing macrophages were present in the uterine endometrial stroma. The other 3 uteri were histologically normal. Multifocal to diffuse positive immunostaining and genomic ISH of the superficial endometrial stroma of the uterus was present as well (Figure 4A and B), with multifocal positive staining in a second female (NHP4). Myometrial smooth muscle was negative in both macaques. TEM demonstrated there were small numbers of viral nucleocapsids forming cytoplasmic tubular and granular inclusions in several cell types, including endometrial stromal cells, fibroblasts and endothelial cells, but not smooth muscle (Figure 4C).

The testis and prostate in the 2 male animals were histologically normal for a sexually immature male (no spermatogenesis). The

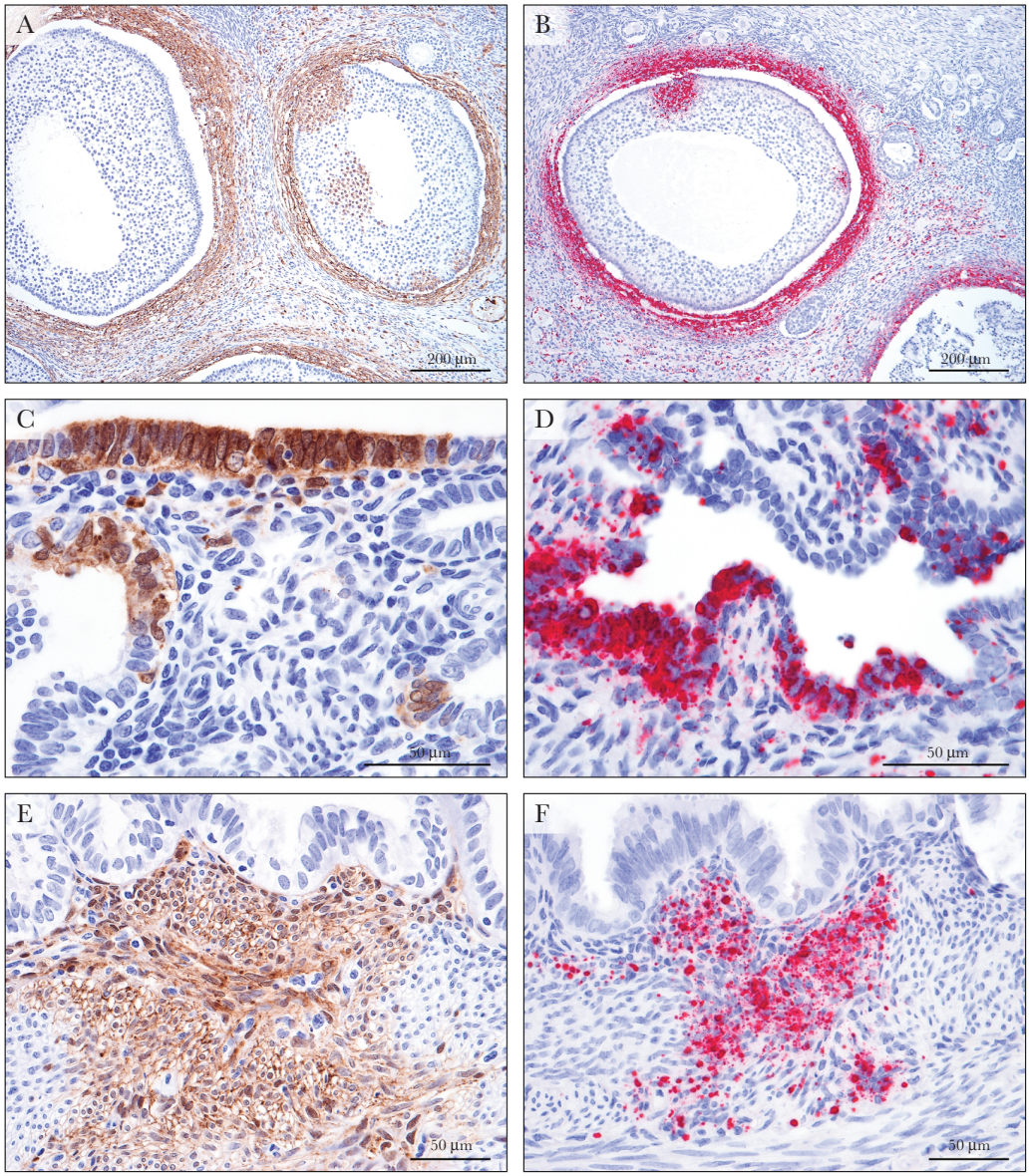

Figure 3. Marburg virus (MARV) localization in the ovaries and oviducts. *A, B,* Cells of the ovarian theca interna surrounding secondary and tertiary follicles are diffusely positive for MARV matrix protein (VP40) and genomic RNA, respectively, with multifocal labeling of granulosa cells and ovarian stromal cells (3,3′-diaminobenzidine [DAB] and red substrate chromagen, respectively, and hematoxylin counterstain). *C, D,* Surface epithelium and subjacent stromal fibroblasts of the endosalpinx of the oviduct express MARV VP40 and contain viral genome. *E, F,* Within the myosalpinx of the oviduct, clusters of smooth muscle cells are positive for MARV VP40 antigen and genomic RNA.

seminal vesicle and bulbourethral gland were also examined in 1 male and were unremarkable. In the testes, IHC- and ISH-positive cells were present the interstitium between seminiferous tubules (Figure 4D and E). Ultrastructurally, viral infection was present in low numbers in the interstitial stromal fibroblasts and endothelial cells between seminiferous tubules only (Figure 4F). In the epididymis, there was positive IHC and ISH staining of few smooth muscle cells surrounding the tubules. IHC, genomic ISH, and TEM, showed that MARV infection in the prostate was present in the interstitium between glands, occasionally associated with small foci of inflammation.

Mammary Glands

The mammary gland was collected incidentally with the axillary lymph node in a single female (NHP3). There was scattered degeneration of acinar cells with rare intracytoplasmic inclusion bodies (Figure 5A). Numerous GP- and VP40-positive epithelial cells were present in the terminal ductules and acini, in addition to interstitial fibroblasts and macrophages (Figure 5B). With ISH, abundant multifocal to coalescing signal was present in acinar and ductal epithelium, and occasionally in lumina of ducts (Figure 5C) and interstitial interacinar fibroblasts and macrophages.

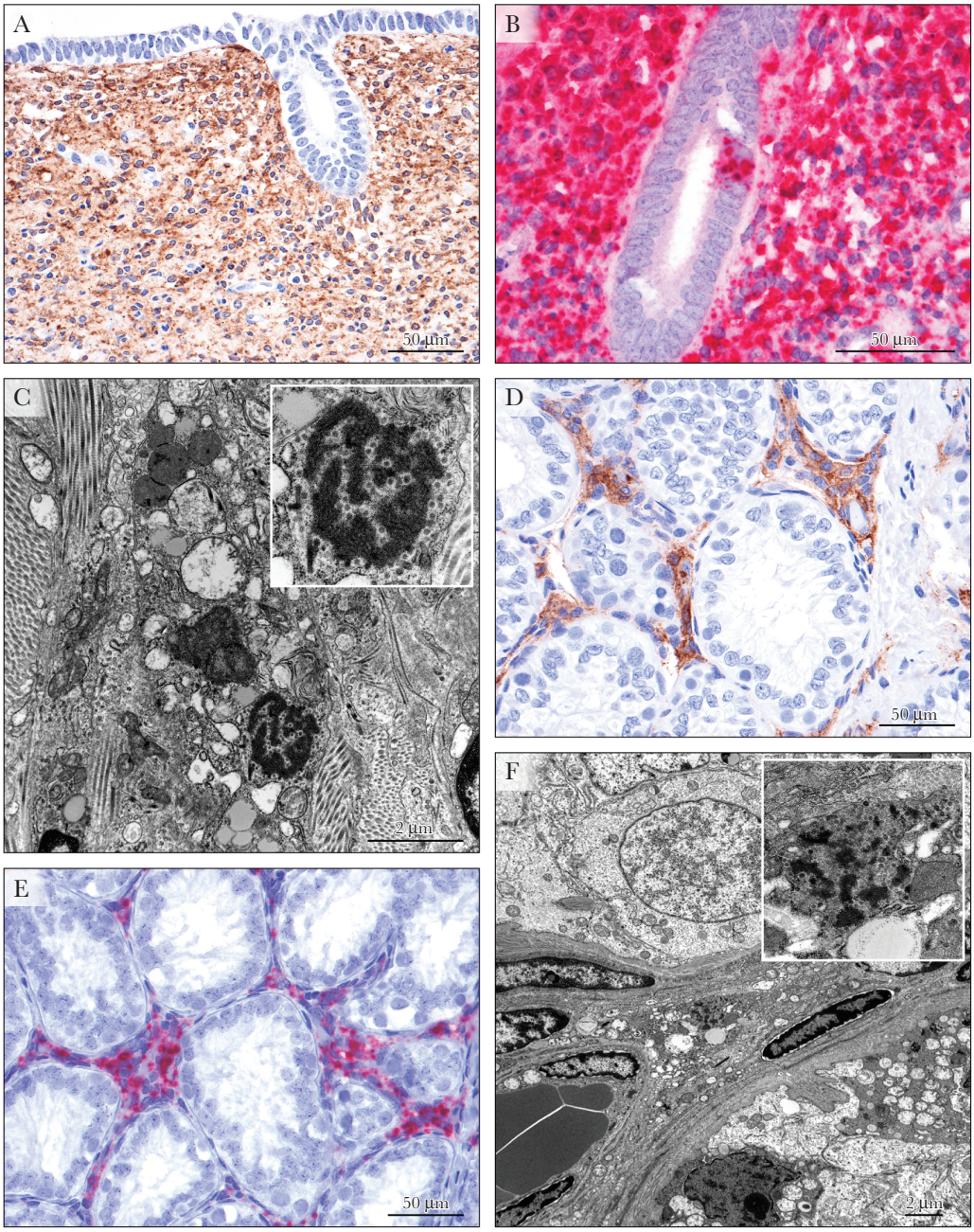

Figure 4. Marburg virus (MARV) localization in the uterus and testis. *A,* The superficial endometrial stroma of the uterus is diffusely positive for MARV matrix protein antigen (3,3′-diaminobenzidine [DAB] chromagen and hematoxylin counterstain). *B,* Strong and diffuse hybridization of viral genome in the endometrial stroma is present with rare labeling of endometrial gland epithelial cells (red substrate chromagen and hematoxylin counterstain). *C,* Ultrastructural appearance shown by transmission electron microscopy (TEM). Intracytoplasmic viral nucleocapsids are present in an endometrial stromal cell, with mature virus particles in the interstitium. Inset shows higher magnification of nucleocapsids. *D,* Testis. The interstitium between seminiferous tubules contains fibroblasts, Leydig cells, and blood vessels, labels for viral glycoprotein. *E,* Scattered labeling of testicular interstitial cells by antigenome in situ hybridization. *F,* TEM shows intracytoplasmic viral nucleocapsids within an interstitial fibroblast in the testis. Inset shows higher magnification of nucleocapsids.

Taste Buds

In the single animal in which taste buds were incidentally collected with the tongue (NHP3), they included frequent apoptotic neuroepithelial cells (Figure 5D). Immunostains and genomic ISH abundantly labeled taste bud neuroepithelium as well as the tongue surface epithelium (Figure 5E and F).

Other Tissues

The thyroid was stained for IHC and ISH in 2 animals (NHP2 and NHP6). In both, approximately 1% of the follicular epithelium stained positively for GP and VP40, with rare positive follicular cells by ISH. The parathyroid of NHP2 also showed scattered small clusters of genomic ISH–positive chief cells not

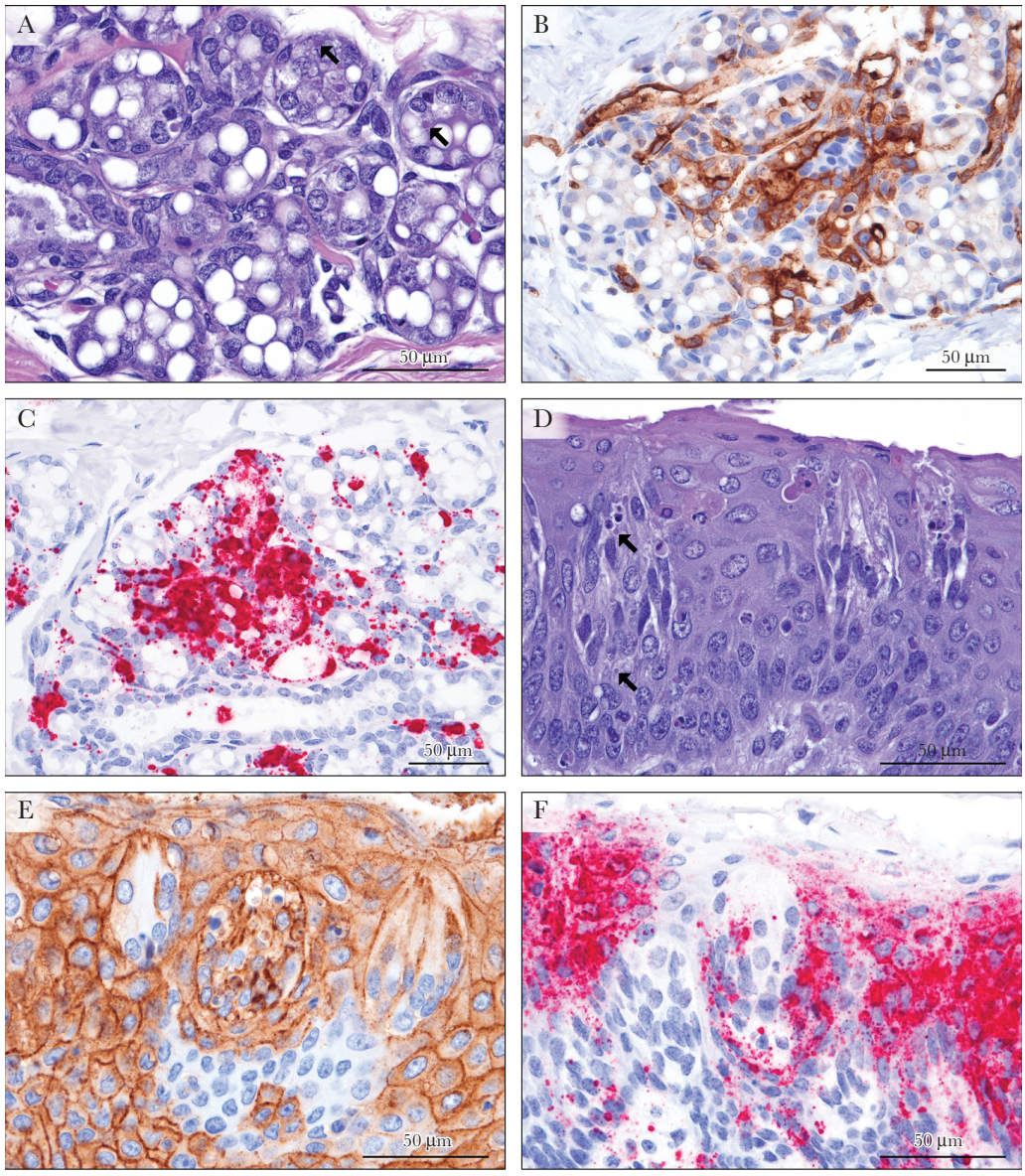

Figure 5. Marburg virus (MARV)–induced changes in mammary glands and tongue. *A*, In the mammary gland, low numbers of degenerate and apoptotic acinar cells are present with rare viral intracytoplasmic inclusion bodies (*arrows*) (hematoxylin-eosin staining). *B*, Immunostaining of MARV glycoprotein (GP) labels mammary acinar and ductal epithelial cells, interstitial fibroblasts, and macrophages (3,3′-diaminobenzidine [DAB] chromagen and hematoxylin counterstain). *C*, Abundant MARV genome is demonstrated by in situ hybridization in the cells and secretions of the mammary gland (red substrate chromagen and hematoxylin counterstain). *D*, Within the circumvallate papilla (tongue), numerous apoptotic cells are within the taste bud and the surface stratified squamous epithelium (Civatte bodies). *E, F*, Neurosensory cells of the taste bud and epithelial cells of the epithelium immunolabel for MARV GP and genome.

seen with IHC. In the submandibular salivary gland, epithelial cell genomic ISH staining was rare in small ducts.

DISCUSSION

This study sought to characterize MARV Angola infection in rhesus macaques, including both major lesions related to fatal course as well as nonfatal lesions with potential long-term consequences. Necropsy was performed after euthanasia in 6 rhesus macaques (*M. mulatta;* 4 female and 2 male) after study end point criteria were met on PIDs 7, 8, and 9. Major findings including clinical signs, clinical pathology changes, and gross and histologic lesions were all consistent with MVD, as reported elsewhere for this model [25–32]. IHC, ISH, and electron microscopic findings confirmed MARV infection targeting cells of the mononuclear phagocytic system and hepatocytes with widespread bystander lymphocyte destruction.

Findings in the eye are intriguing with regard to long-term disease, either from persistence of the virus, because the eye is considered an immune-privileged site, or from sterile postinfection inflammation and/or scarring. EBOV

infection of the eye is reported to only appear late in the disease course in macaques (PID >14), and the ciliary body and iris (anterior uvea) are important sites of infection/inflammation within the eyes of both humans and macaques [33–36]. Similar to EBOV, uveitis has also been reported in human survivors of MVD [19, 37].

In 3 of 6 animals euthanatized at PID 7, 8, or 9, there were already histologically identifiable minimal macrophage infiltrates into the stroma of the iris (iriditis/anterior uveitis). In addition, MARV was demonstrated by IHC and ISH in the iris and ciliary body in 5 and 6 animals, respectively, even at this relatively early stage of infection. The ciliary body secretes the aqueous humor necessary for nourishing the avascular lens and maintaining normal intraocular pressure, and ocular hypotony (reduced intraocular pressures) and cataracts have been noted in EVD survivors [36]. Emboli of necrotic macrophages occluding uveal vessels could result in ischemic necrosis and/or inflammation of the adjacent delicate neuroretina, resulting in retinal scarring [36]. The presence of virus in such an immunoprivileged site creates the potential not only for chronic local inflammation and disease but also for systemic dissemination and recrudescence [37].

In 2 animals, viral RNA was also identified multifocally in the inner nuclear cell layer of the retina. This layer consists of predominantly bipolar integrating neurons, with fewer unipolar amacrine cells (inhibitory neurons) and Müller (glial) cells. Leakage of virus from vasculature is suspected, although no hemorrhage or edema was present. Filovirus infection of neurons during acute disease is considered controversial and has not been previously reported [33]. Filovirus within the neuroretina has not been previously identified, although researchers have speculated that EBOV could be within the ganglion cells of the inner retina [38].

Lesions in the peripheral nerves and ganglia may be germane to altered peripheral nerve and autonomic nervous system functions reported in EVD and MVD survivors [2, 7, 39, 40]. Paresthesia and hyperaesthesia have been reported in patients with MVD during acute infection as well [3]. Inflammation and destruction of these tissues has the potential for long-term functional consequences such as parasthesias, dysthesias, or autonomic dysfunction. Destruction of peripheral nerve axon(s) could result in temporary loss of transmission in the case of Wallerian degeneration with successful nerve regrowth, or permanent loss or abnormal sensation (neuroma) if axonal regrowth is unsuccessful. Damage to the supporting cells of the myelinated nerves, including the Schwann cells that make and maintain the myelin sheath, could result in demyelination, with or without secondary destruction of the nerve axon. Such damage could uncover cryptic autoantigens, leading to immune-mediated disease.

A similar spectrum of lesions was noted in incidentally collected peripheral parasympathetic autonomic ganglia, and could contribute to dysautonomia syndromes, including altered gastrointestinal motility and function. With specific regard to the submandibular (Langley's) ganglion, parasympathetic stimulation of the salivary glands results in secretion of serous saliva and ions. Damage to this ganglion could cause dry mouth (xerostomia) and difficulty swallowing, complications noted in EVD survivors [7]. Xerostomia also contributes to dental caries, thereby potentially negatively affecting appetite and nutrition. Similar lesions in the peripheral ganglia and nerves have recently been reported in the guinea pig acute EBOV infection model [23]. Related to this, viral infection of the taste buds would cause temporary loss of sensation if only the sensory neuroepithelial cells were affected but would be permanent with destruction of basal stem cells. Altered or diminished taste has been reported in EVD survivors as well and could potentially contribute to anorexia and malnutrition [7].

Histologic, IHC, ISH, and ultrastructural findings in the gonads and genital tract are similar to those seen in the rhesus macaque acute EBOV model [24]. Ovarian and testicular necrotizing lesions have been reported from autopsies of humans dying of MARV infection [2]. Although sexual transmission of EBOV and MARV in semen has been documented [2, 41, 42], there was no evidence of viral contamination of seminal fluid in this study. However, only 2 males were included, and both were sexually immature with no active spermatogenesis. Long-term sequelae, including potential sexual and vertical transmission, abortion, and potential viral recrudescence in pregnancy, are areas requiring further study in filovirus disease. The presence of viral antigen and genome in the epithelial cells and secretions of the mammary gland in this study is of potential interest, as the transmission of virus in human breast milk is suspected during prodromal and acute infections with MARV and EBOV [16, 43, 44]. Further study of MARV infection in pregnant and lactating female macaques could be of great utility [45, 46].

Viral infection of the pancreatic endocrine islets of Langerhans and adrenal cortex (and medulla) was reported elsewhere in rhesus macaques infected with this MARV isolate [25]. Infection of adrenal and islet cells was reported in spontaneous human MVD cases as well [47]. Adrenal cortical cells were also immunostained in cynomolgus macaques infected with the MARV Ci67 isolate [48]. Infection of the thyroid follicular epithelium has not been documented in the macaque MARV model, although foci of thyroid necrosis were noted in human victims of the original 1967 outbreak [28, 49]. Viral infection of the follicular epithelium with necrosis has been noted elsewhere in the rhesus macaque EBOV infection models in animals with a prolonged clinical course, and recently in the guinea pig acute EBOV infection model [23, 34]. Infection of parathyroid chief cells has not been previously noted with either EVD or MVD in macaques, humans, or guinea pigs.

Despite 50 years of experience with MARV since its first recognition, including experimental infection in the rhesus

macaque model, the pathophysiology and cell tropism of this and related viruses remain incompletely understood. Although long-term complications had been observed in survivors of MVD as early as the first outbreak, the unprecedented number of survivors from the 2013–2016 West African epidemic, combined with continued sporadic incursions of MARV and EBOV in Africa [50–52], provide new urgency to studying the pathogenesis of these sequela. The potential for different virus doses and routes of infection to model a less lethal spectrum of disease is one potential avenue of investigation, both by potentially producing a prolonged course of disease as well as by creating survivors of MVD [53, 54]. Herein we have shown viral targeting of a number of not previously recognized tissues and cell types, which are highly relevant for observed postinfection disease of both MVD and EVD. Although a faithful survivor animal model of MVD complications is needed, the findings reported here should inform future studies of MVD sequelae in acute and chronic models.

Supplementary Data

Supplementary materials are available at *The Journal of Infectious Diseases* online. Consisting of data provided by the authors to benefit the reader, the posted materials are not copyedited and are the sole responsibility of the authors, so questions or comments should be addressed to the corresponding author.

Notes

Acknowledgments. We thank Donna L. Perry, DVM, PhD, for gross necropsy and tissue collection and Louis Huzella, DVM, Donna L. Perry, and Mike Holbrook, PhD, for manuscript review. Rebecca Shim, Mason Waters, Kyra Hadley, Brittany Brockett, and Bonnie Dighero-Kemp performed clinical pathologic testing. Ricky Adams and Tracey Burdette performed virus plaque assays and quantitative reverse-transcriptase polymerase chain reaction. We thank Laura Bollinger for technical writing services and Jiro Wada for figure preparation.

Disclaimer. The findings and conclusions in this report are those of the authors and do not necessarily reflect the views or policies of the US Department of Health and Human Services or of the institutions and companies affiliated with the authors.

Financial support. This work was supported by the Division of Intramural Research of the National Institute of Allergy and Infectious Diseases (NIAID); Integrated Research Facility (NIAID, Division of Clinical Research); and Battelle Memorial Institute's prime contract with NIAID (Contract # HHSN272200700016I).

Potential conflicts of interest. All authors: No potential conflicts. All authors have submitted the ICMJE Form for Disclosure of Potential Conflicts of Interest. Conflicts that are considered relevant to the content of the manuscript have been disclosed.

References

1. Feldmann H, Sanchez A, Geisbert TW. Filoviridae: Marburg and Ebola viruses. In: Knipe D, Howley P, eds. Fields virology. 6th ed. Vol 2. Philadelphia, PA: Lippincott Williams and Wilkins, **2013**:923–56.
2. Martini GA. Marburg virus disease. Postgrad Med J **1973**; 49:542–6.
3. Martini GA. Marburg virus disease: clinical syndrome. In: Martini GA, Siegert R, eds. Marburg virus disease. Berlin, Germany: Springer-Verlag, **1971**:1–9.
4. World Health Organization. Ebola situation report—30 March 2016. http://apps.who.int/ebola/current-situation/ebola-situation-report-30-march-2016. Accessed 10 January 2018.
5. National Institute of Allergy and Infectious Diseases, National Library of Medicine. Ebola virus disease survivors: clinical and immunologic follow-up. ClinicalTrials.gov identifier: NCT02431923. https://clinicaltrials.gov/ct2/show/NCT02431923?term=prevail&cond=Ebola+Virus+Disease&rank=5. Accessed 10 January 2018.
6. World Health Organization. Clinical care for survivors of Ebola virus disease. http://www.who.int/csr/resources/publications/ebola/guidance-survivors/en/. Accessed 5 January 2018.
7. Bennett RS, Huzella LM, Jahrling PB, Bollinger L, Olinger GG Jr, Hensley LE. Nonhuman primate models of Ebola virus disease. Curr Top Microbiol Immunol **2017**; 411:171–93.
8. Rowe AK, Bertolli J, Khan AS, et al; Commission de Lutte contre les Epidémies à Kikwit. Clinical, virologic, and immunologic follow-up of convalescent Ebola hemorrhagic fever patients and their household contacts, Kikwit, Democratic Republic of the Congo. J Infect Dis **1999**; 179(suppl 1):S28–35.
9. Jeffs B, Roddy P, Weatherill D, et al. The Medecins Sans Frontieres intervention in the Marburg hemorrhagic fever epidemic, Uige, Angola, 2005. I. Lessons learned in the hospital. J Infect Dis **2007**; 196(suppl 2):S154–61.
10. Towner JS, Pourrut X, Albariño CG, et al. Marburg virus infection detected in a common African bat. PLoS One **2007**; 2:e764.
11. Centers for Disease Control and Prevention. Marburg hemorrhagic fever. https://www.cdc.gov/vhf/marburg/index.html. Accessed 5 January 2018.
12. Martini GA, Knauff HG, Schmidt HA, Mayer G, Baltzer G. On the hitherto unknown, in monkeys originating infectious disease: Marburg virus disease. Dtsch Med Wochenschr **1968**; 93:559–71.
13. World Health Organization. Marburg virus disease. Fact sheet. http://www.who.int/mediacentre/factsheets/fs_marburg/en/. Accessed 5 January 2018.
14. Weidmann M, Hufert FT, Sall AA. Viral load among patients infected with Marburgvirus in Angola. J Clin Virol **2007**; 39:65–6.
15. Martines RB, Ng DL, Greer PW, Rollin PE, Zaki SR. Tissue and cellular tropism, pathology and pathogenesis of Ebola and Marburg viruses. J Pathol **2015**; 235:153–74.
16. Borchert M, Muyembe-Tamfum JJ, Colebunders R, Libande M, Sabue M, Van Der Stuyft P. Short communication: a cluster of Marburg virus disease involving an infant. Trop Med Int Health **2002**; 7:902–6.
17. Martini GA, Schmidt HA. Spermatogenic transmission of the "Marburg virus" (causes of "Marburg simian disease") [in German]. Klin Wochenschr **1968**; 46:398–400.
18. Stille W, Boehle E. Clinical course and prognosis of Marburg virus ("green-monkey") disease. In: Martini GA, Siegert R, eds. Marburg virus disease. Berlin, Germany: Springer-Verlag, **1971**:10–8.
19. Gear JS, Cassel GA, Gear AJ, et al. Outbreake of Marburg virus disease in Johannesburg. Br Med J **1975**; 4:489–93.
20. Mehedi M, Groseth A, Feldmann H, Ebihara H. Clinical aspects of Marburg hemorrhagic fever. Future Virol **2011**; 6:1091–106.
21. Honko AN, Johnson JC, Marchand JS, et al. High dose sertraline monotherapy fails to protect rhesus macaques from lethal challenge with Ebola virus Makona. Sci Rep **2017**; 7:5886.
22. Guide for the care and use of laboratory animals, 8th ed. Washington, DC: The National Academies Press, **2011**.
23. Cooper TK, Huzella L, Johnson JC, et al. Histology, immunohistochemistry, and in situ hybridization reveal overlooked Ebola virus target tissues in the Ebola virus disease guinea pig model. Sci Rep **2018**; 8:1250.
24. Perry DL, Huzella LM, Bernbaum JG, et al. Ebola virus localization in the macaque reproductive tract during acute Ebola virus disease. Am J Pathol **2018**; 188:550–8.
25. Geisbert TW, Daddario-DiCaprio KM, Geisbert JB, et al. Marburg virus Angola infection of rhesus macaques: pathogenesis and treatment with recombinant nematode anticoagulant protein c2. J Infect Dis **2007**; 196(suppl 2):S372–81.
26. Johnston SC, Lin KL, Twenhafel NA, et al. Dose response of MARV/Angola infection in cynomolgus macaques following IM or aerosol exposure. PLoS One **2015**; 10:e0138843.
27. Daddario-DiCaprio KM, Geisbert TW, Ströher U, et al. Postexposure protection against Marburg haemorrhagic fever with recombinant vesicular stomatitis virus vectors in non-human primates: an efficacy assessment. Lancet **2006**; 367:1399–404.
28. Zlotnik I. Marburg agent disease: pathology. Trans R Soc Trop Med Hyg **1969**; 63:310–27.

29. Simpson DI, Zlotnik I, Rutter DA. Vervet monkey disease: experiment infection of guinea pigs and monkeys with the causative agent. Br J Exp Pathol **1968**; 49:458–64.
30. Thi EP, Mire CE, Ursic-Bedoya R, et al. Marburg virus infection in nonhuman primates: therapeutic treatment by lipid-encapsulated siRNA. Sci Transl Med **2014**; 6:250ra116.
31. Alves DA, Glynn AR, Steele KE, et al. Aerosol exposure to the Angola strain of Marburg virus causes lethal viral hemorrhagic fever in cynomolgus macaques. Vet Pathol **2010**; 47:831–51.
32. Glaze ER, Roy MJ, Dalrymple LW, Lanning LL. A comparison of the pathogenesis of Marburg virus disease in humans and nonhuman primates and evaluation of the suitability of these animal models for predicting clinical efficacy under the 'animal rule.' Comp Med **2015**; 65:241–59.
33. Zeng X, Blancett CD, Koistinen KA, et al. Identification and pathological characterization of persistent asymptomatic Ebola virus infection in rhesus monkeys. Nat Microbiol **2017**; 2:17113.
34. Larsen T, Stevens EL, Davis KJ, et al. Pathologic findings associated with delayed death in nonhuman primates experimentally infected with Zaire Ebola virus. J Infect Dis **2007**; 196(suppl 2):S323–8.
35. Alves DA, Honko AN, Kortepeter MG, et al. Necrotizing scleritis, conjunctivitis, and other pathologic findings in the left eye and brain of an Ebola virus-infected rhesus Macaque (*Macaca mulatta*) with apparent recovery and a delayed time of death. J Infect Dis **2016**; 213:57–60.
36. Shantha JG, Crozier I, Yeh S. An update on ocular complications of Ebola virus disease. Curr Opin Ophthalmol **2017**; 28:600–6.
37. Kuming BS, Kokoris N. Uveal involvement in Marburg virus disease. Br J Ophthalmol **1977**; 61:265–6.
38. Steptoe PJ, Scott JT, Baxter JM, et al. Novel retinal lesion in Ebola survivors, Sierra Leone, 2016. Emerg Infect Dis **2017**; 23:1102–9.
39. Tiffany A, Vetter P, Mattia J, et al. Ebola virus disease complications as experienced by survivors in Sierra Leone. Clin Infect Dis **2016**; 62:1360–6.
40. Slenczka W, Klenk HD. Forty years of Marburg virus. J Infect Dis **2007**; 196(suppl 2):S131–5.
41. Christie A, Davies-Wayne GJ, Cordier-Lassalle T, et al; Centers for Disease Control and Prevention (CDC). Possible sexual transmission of Ebola virus—Liberia, 2015. MMWR Morb Mortal Wkly Rep **2015**; 64:479–81.
42. Diallo B, Sissoko D, Loman NJ, et al. Resurgence of Ebola virus disease in guinea linked to a survivor with virus persistence in seminal fluid for more than 500 days. Clin Infect Dis **2016**; 63:1353–6.
43. Grolla A, Jones SM, Fernando L, et al. The use of a mobile laboratory unit in support of patient management and epidemiological surveillance during the 2005 Marburg outbreak in Angola. PLoS Negl Trop Dis **2011**; 5:e1183.
44. Sissoko D, Keïta M, Diallo B, et al. Ebola virus persistence in breast milk after no reported illness: a likely source of virus transmission from mother to child. Clin Infect Dis **2017**; 64:513–6.
45. Bebell LM, Oduyebo T, Riley LE. Ebola virus disease and pregnancy: a review of the current knowledge of Ebola virus pathogenesis, maternal, and neonatal outcomes. Birth Defects Res **2017**; 109:353–62.
46. Henwood PC, Bebell LM, Roshania R, et al. Ebola virus disease and pregnancy: a retrospective cohort study of patients managed at 5 Ebola treatment Units in West Africa. Clin Infect Dis **2017**; 65:292–9.
47. Geisbert TW, Jaax NK. Marburg hemorrhagic fever: report of a case studied by immunohistochemistry and electron microscopy. Ultrastruct Pathol **1998**; 22:3–17.
48. Hensley LE, Alves DA, Geisbert JB, et al. Pathogenesis of Marburg hemorrhagic fever in cynomolgus macaques. J Infect Dis **2011**; 204(suppl 3):S1021–31.
49. Gedigk P, Bechtelsheimer H, Korb G. Pathological anatomy of the "Marburg virus" disease (the so-called "Marburg monkey disease") [in German]. Dtsch Med Wochenschr **1968**; 93:590–601.
50. Wasswa H. Uganda grapples with new Marburg disease outbreak. BMJ **2017**; 359:j5252.
51. Nyakarahuka L, Ojwang J, Tumusiime A, et al. Isolated case of Marburg virus disease, Kampala, Uganda, 2014. Emerg Infect Dis **2017**; 23:1001–4.
52. Green A. Ebola outbreak in the DR Congo. Lancet **2017**; 389:2092.
53. Speranza E, Bixler SL, Altamura LA, et al. A conserved transcriptional response to intranasal Ebola virus exposure in nonhuman primates prior to onset of fever. Sci Transl Med **2018**; 10:eaaq1016. doi:10.1126/scitranslmed.aaq1016.
54. Bray M, Hatfill S, Hensley L, Huggins JW. Haematological, biochemical and coagulation changes in mice, guinea-pigs and monkeys infected with a mouse-adapted variant of Ebola Zaire virus. J Comp Pathol **2001**; 125:243–53.